

2.5-MHD models of circumstellar discs around FS CMa post-mergers : II. Stationary accretion stage

A. Moranchel-Basurto,^{1*} D. Korčáková,¹ and R. O. Chametla¹

¹Charles University, Faculty of Mathematics and Physics, Astronomical Institute, V Holešovičkách 747/2, 180 00 Prague 8, Czech Republic

Accepted XXX. Received YYY; in original form ZZZ

ABSTRACT

We study the star-disc interaction in the presence of the strong magnetic field ($B_{\star} = 6.2kG$) of a slowly rotating star. This situation describes a post-merger of the spectral type B and has not been previously investigated. We perform a set of resistive and viscosity 2.5D-magnetohydrodynamical simulations using the PLUTO code. Based on our previous work, we consider the initial gas disc density $\rho_{d0} = 10^{-13} \text{gcm}^{-3}$ since it describes the conditions around IRAS 17449+2320 well. We find that the fall of gas towards the star occurs in the mid-plane, and remarkably, intermittent backflow takes place in the mid-plane in all of our models for $R \geq 10R_{\star}$. However, we do not rule out that the funnel effect may occur and cause the accretion closer to the poles. Also, when larger values of viscosity ($\alpha_{\nu} = 1$) and stellar rotation rate ($\delta_{\star} = 0.2$) are considered, we find that the disc exhibits a thickening which is characteristic of FS CMa-type stellar objects. Additionally, we find that the poloidal magnetic field lines twist over short periods of time, leading to magnetic reconnection causing coronal heating that could explain the presence of the Raman lines found observationally in several FS CMa stars. Lastly, we find the formation of several knots in the magnetic field lines near and in the mid-plane of the disc which produce perturbations in the density and velocity components, as well as the formation of shallow gaps whose position depends on the inflation of the magnetic field lines.

Key words: stars:magnetic fields – accretion, accretion discs – methods:numerical magnetohydrodynamics (MHD)

1 INTRODUCTION

In the recent two decades the theoretical and numerical effort to understand the dynamics of gas during the interaction between the magnetosphere and the inner region of an accretion disc of a rotating-magnetized star has produced important advances for some types of stars such as: classical T Tauri stars, white dwarfs, neutron stars, X-ray pulsars, among others (Koldoba et al. 2002; Romanova et al. 2002; Long et al. 2005; Bessolaz et al. 2008; Kluźniak & Rappaport 2007; Zanni & Ferreira 2009, 2013; Čemeljić 2019; Ireland et al. 2021; Čemeljić et al. 2023). Among the most important results are the bounding of the disc truncation radius value due to the star’s magnetosphere and the formation of accretion funnel flows. The latter is implicitly associated with the spin-up torque felt by the star and represents a stationary gas accretion state. However, both outcomes remain in the regime of sun-like mass stars including a weak magnetic field ($B_{\star} \leq 1kG$).

Less studied is the star magnetosphere-disc interaction regime for more massive stars with a strong magnetic field (Miller & Stone 1997; Moranchel-Basurto et al. 2023; Čemeljić et al. 2023). Apart from the expensive computational cost, the study of this type of interaction represents a complex problem itself, as has been well pointed out in Moranchel-Basurto et al. (2023, hereinafter called Paper I), since very strong magnetic field coming from the central star can produce a highly dynamic accretion of gas (non-stationary stage).

It is worth mentioning that the stationary or non-stationary regime of the accretion depends mostly on the initial conditions and the strength of the magnetic field does not play the crucial role. Therefore, being able to restrict the free parameters to the smallest possible number can make the study of the interaction of the magnetosphere with the inner disc more tractable, at least in numerical models. For instance, Čemeljić (2019) studied star-disc magnetospheric interaction (including only a high viscosity in the disc, $\alpha_{\nu} = 1$) by an ‘Atlas’ of numerical models trying to obtain quasi-stationary solutions which can be applied to accretion discs around of the YSO-type objects with a low magnetic field ($B_{\star} < 1kG$). He found that increasing stellar magnetic field in the simulation, the gas density of the disc increases. Furthermore, he found that in models with a faster rotation of the star, additional solutions are produced: (i) a fast axial outflow, and, (ii) with both the conical and axial outflow, similar to what was reported in Romanova et al. (2009).

With all the above in mind, the parameters obtained from the observations play an important role. Within the regime of massive stars with a strong magnetic field are the objects called FS CMa post-mergers. Particular attention must be paid to the member of this set labeled as IRAS 17449+2320 object. Because in a recent study the magnitude of the magnetic field on the surface of the star was determined ($B_{\star} = 6.2kG$; see Korčáková et al. 2022, and Paper I for details). So, similar to Paper I, we are interested in studying the star-disc magnetosphere interaction in said regime taking into account the observational parameters for the FS CMa stars, such as: the mass ($M_{\star} = 6M_{\odot}$) and stellar radius ($R_{\star} = 3R_{\odot}$) (Kříček

* E-mail: amoranchel087@gmail.com

et al. 2017), and the value of the magnetic field mentioned above. Nevertheless, in this case with the aim of seeing if the stationary accretion stage takes place, unlike Paper I, here we include as free parameters the stellar rotation rate δ_\star , the magnetic diffusivity α_m and the viscosity α_ν within the disc in our numerical models.

The paper is laid out as follows. In Section 2 we present the physical model, while the numerical implementations used in our 2.5D magnetohydrodynamical simulations are discussed in section 3. In Section 4 we present the results of our numerical models. A brief discussion is presented in Section 5 and finally concluding remarks can be found in Section 6.

2 PHYSICAL MODEL

Our physical model is composed of a slightly sub-Keplerian disc around a magnetized rotating star with a dipolar magnetic field configuration. The models presented in this study are numerical solutions of the magnetohydrodynamical (MHD) equations in which the effects of viscosity and resistivity within the disc are taken into account. Apart from the free parameters considered in this study, our physical model follows those presented in Paper I.

2.1 MHD equations

The magnetohydrodynamic equations governing the gas dynamics are the conservation of mass

$$\frac{\partial \rho}{\partial t} + \nabla \cdot (\rho \mathbf{v}) = 0, \quad (1)$$

the conservation of momentum equation

$$\frac{\partial \rho \mathbf{v}}{\partial t} + \nabla \cdot \left[\rho \mathbf{v} \mathbf{v} + \left(P + \frac{\mathbf{B} \cdot \mathbf{B}}{8\pi} \right) \mathbf{I} - \frac{\mathbf{B} \mathbf{B}}{4\pi} - \tau \right] = -\rho \nabla \Phi, \quad (2)$$

the energy equation

$$\begin{aligned} \frac{\partial E}{\partial t} + \nabla \cdot \left[\mathbf{v} \left(E + P + \frac{\mathbf{B} \cdot \mathbf{B}}{8\pi} \right) - \frac{1}{4\pi} (\mathbf{v} \cdot \mathbf{B}) \mathbf{B} \right] \\ + \nabla \cdot \left(\eta_m \mathbf{J} \times \frac{\mathbf{B}}{4\pi} - \mathbf{v} \cdot \tau \right) = -\rho (\nabla \Phi) \cdot \mathbf{v} - \Lambda_{cool}, \end{aligned} \quad (3)$$

the last term on the left side of the energy equation (3) includes the heating terms, to balance this, note that the cooling term Λ_{cool} has been included on the right side of the equation, that means, that the system should evolve adiabatically. Said cooling term also helps prevent the thermal thickening of the gas disc (Zanni & Ferreira 2009).

And finally the induction equation by which the description of the evolution of the magnetic field is described is given by:

$$\frac{\partial \mathbf{B}}{\partial t} - \nabla \times (\mathbf{v} \times \mathbf{B} - \eta_m \mathbf{J}) = 0. \quad (4)$$

where P is the thermal gas pressure, ρ the gas density, \mathbf{v} its velocity, \mathbf{I} the unit tensor, \mathbf{B} the magnetic flux density vector, \mathbf{J} is the electric current density given by the Ampère's law $\mathbf{J} = \nabla \times \mathbf{B}/4\pi$, η_m is the resistivity and is related with the magnetic diffusivity by $\nu_m = \eta_m/4\pi$, $\Phi = GM_\star/R$ the gravitational potential and E represents the total energy density given by

$$E = \frac{P}{\gamma - 1} + \rho \frac{\mathbf{v} \cdot \mathbf{v}}{2} + \frac{\mathbf{B} \cdot \mathbf{B}}{8\pi}, \quad (5)$$

where $\gamma = 5/3$ is the polytropic index of the plasma. On the other hand, the viscous stress tensor τ is defined as:

$$\tau = \eta_\nu \left[(\nabla \mathbf{v}) + (\nabla \mathbf{v})^T - \frac{2}{3} (\nabla \cdot \mathbf{v}) \mathbf{I} \right], \quad (6)$$

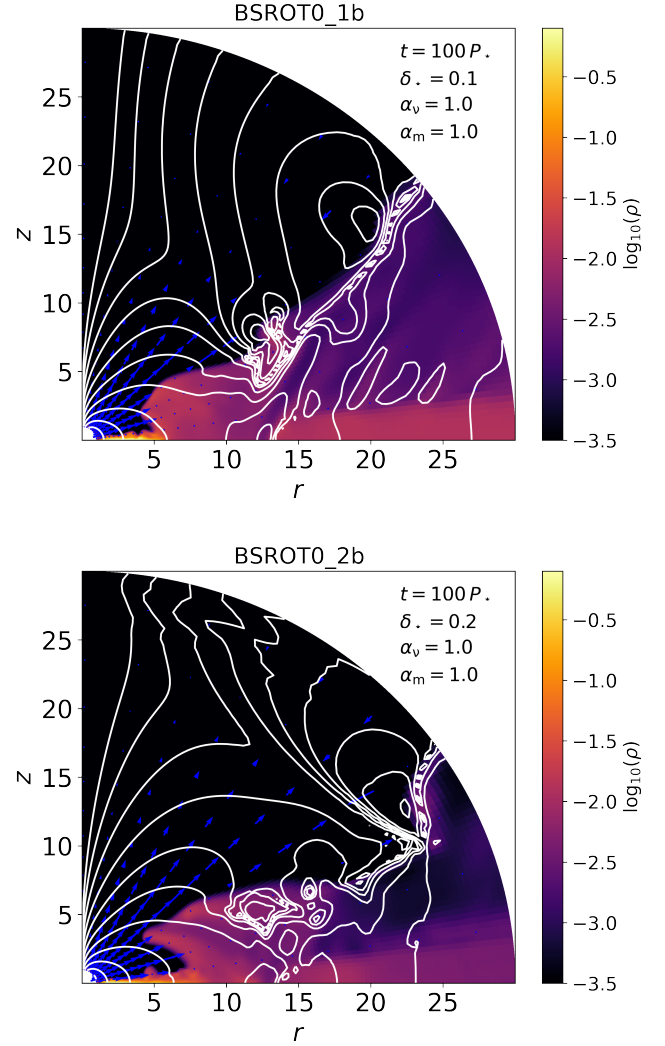


Figure 1. Upper panel shows logarithmic gas density for the BSROT_1b model with a low rate of stellar rotation $\delta_\star \equiv \Omega_\star/\Omega_{br} = 0.1$. It can be seen the formation of the funnel effect as well as the formation of disc winds and magnetospheric ejections. Bottom panel shows logarithmic gas density for the BSROT_2b model with a higher rate of stellar rotation $\delta_\star = 0.2$. In this case we find the formation of multiple disc layers between $r = 5r_0$ and $r = 10r_0$ as well as the inflation of the disc that resembles the formation of a huge funnel. The white lines show the poloidal magnetic field lines. Note that in both models except for the increase in the stellar rotation rate in a factor 2, all other parameters remained fixed.

where η_ν is the dynamic and $\nu_\nu = \eta_\nu/\rho$ the kinematic viscosity, respectively.

2.2 Accretion disc

The density ρ_d and pressure P_d of the gas in the accretion disc is set following the three-dimensional models of Keplerian accretion discs considering spherical coordinates (R, θ, ϕ) used in Zanni & Ferreira (2009) (which in turn is based on the disc model of Kluzniak & Kita 2000):

$$\rho_d(R, r) = \rho_{d0} \left\{ \frac{2}{5h^2} \left[\frac{R_0}{R} - \left(1 - \frac{5h^2}{2} \right) \frac{R_0}{r} \right] \right\}^{3/2}, \quad (7)$$

$$P_d = h^2 \rho_{d0} v_{K0}^2 \left(\frac{\rho_d}{\rho_{d0}} \right)^{5/3} \quad (8)$$

where $h = C_s/v_K$ is the aspect ratio, with C_s and $v_K = \sqrt{GM_*/R}$ the sound speed and the Keplerian velocity, respectively. In Eq. (7) ρ_{d0} and v_{K0} denote the initial values of the density and the Keplerian velocity calculated at $R = R_0$ in the mid-plane of the disc. Note that we define $r = R \sin \theta$ as the cylindrical radius.

The velocity components ($u_{Rd}, u_{\theta d}, u_{\phi d}$) of the accretion disc are calculated as (Kluźniak & Kita 2000; Zanni & Ferreira 2009, 2013; Ćemeljić 2019):

$$u_{Rd} = -\alpha_v h^2 \left[10 - \frac{32}{3} \Lambda \alpha_v^2 - \Lambda \left(5 - \frac{1}{h^2 \tan^2 \theta} \right) \right] \sqrt{\frac{GM_*}{R \sin^3 \theta}}, \quad (9)$$

$$u_{\phi d} = \left[\sqrt{1 - \frac{5h^2}{2}} + \frac{2}{3} h^2 \alpha_v^2 \Lambda \left(1 - \frac{6}{5h^2 \tan^2 \theta} \right) \right] \sqrt{\frac{GM_*}{r}}, \quad (10)$$

$$u_{\theta d} = 0. \quad (11)$$

In Eqs (9-10), $\Lambda = (11/5)/(1 + 64\alpha_v^2/25)$. Note that we are considering a slightly sub-Keplerian disc.

2.3 Disc atmosphere

In a similar form to Zanni & Ferreira (2009), we included a non-rotating polytropic hydrostatic atmosphere with a density

$$\rho_{\text{atm}}(R) = \rho_{\text{atm}}^0 \left(\frac{R_*}{R} \right)^{\frac{1}{\gamma-1}} \quad (12)$$

and pressure

$$P_{\text{atm}}(R) = \rho_{\text{atm}}^0 \frac{\gamma-1}{\gamma} \frac{GM_*}{R_*} \left(\frac{R_*}{R} \right)^{\frac{\gamma}{\gamma-1}} \quad (13)$$

with $\gamma = 5/3$. The density contrast between the disc and the atmosphere is $\rho_{\text{atm}}^0/\rho_{d0} = 0.01$, which is kept fixed in all our models.

2.4 Magnetic field configuration

We assume that the star is located at the origin of the coordinate system. The stellar magnetosphere is modeled initially as a purely dipolar field aligned with the rotation axis of the star-disc system. The magnetic field is defined by the flux function Ψ_*

$$\Psi_*(R, \theta) = B_* R_*^3 \frac{\sin^2 \theta}{R} \quad (14)$$

where B_* is the magnetic field at R_* and $z = 0$. The radial and polar field components are therefore given respectively by

$$B_R = \frac{1}{R^2 \sin \theta} \frac{\partial \Psi_*}{\partial \theta} \quad (15)$$

and

$$B_\theta = -\frac{1}{R \sin \theta} \frac{\partial \Psi_*}{\partial R}. \quad (16)$$

The relation between flux function and potential vector is given by:

$$\Psi_* = R A_\phi \sin \theta \quad (17)$$

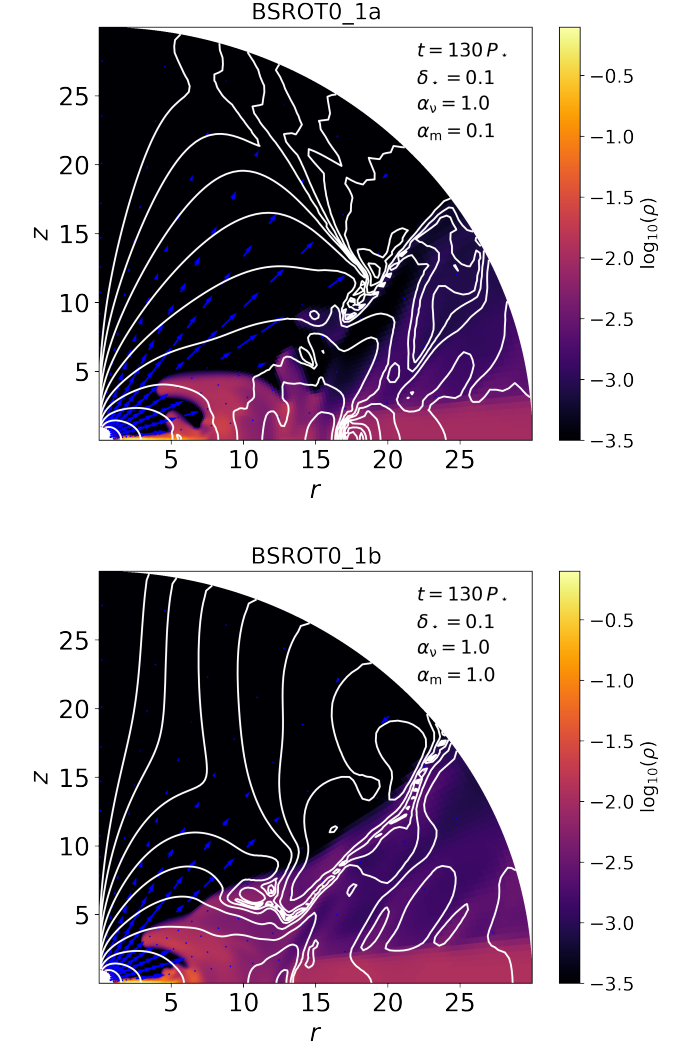


Figure 2. Upper panel shows logarithmic gas density for the BSROT_1a model with a low rate of stellar rotation $\delta_* = 0.1$ as well as a low magnetic diffusivity $\alpha_m = 0.1$. Bottom panel shows logarithmic gas density for the BSROT_1b model with a higher magnetic diffusivity $\alpha_m = 1.0$. The white lines show the poloidal magnetic field lines.

and then the components of potential vector in spherical coordinates are given by:

$$A_\phi(R, \theta) = \frac{B_* R_*^3 \sin \theta}{R^2}, \quad (18)$$

$A_R = 0$ and $A_\theta = 0$.

It should be noted that for a suitable numerical treatment of the magnetic field, we employ the “field-splitting” technique (Tanaka 1994; Powell et al. 1999) which is widely used in this type of studies (see Ćemeljić 2019, and references therein).

2.5 Magnetic diffusivity models

The role of magnetic diffusivity ν_m can be important, this can arise from turbulence generated in the disc and this parameter may be responsible for modifying the strength of the magnetic field lines. For this reason we decided to explore different descriptions of resistivity

$\eta_m = 4\pi\nu_m$, considering that the magnetic diffusivity ν_m is given by:

- Classical description (Zanni & Ferreira 2009; Čemeljić 2019):

$$\nu_m = \frac{\alpha_m C_s^2}{\Omega_K} \quad (19)$$

- Modified first version (see Masoumeh & Khesali 2022, and references therein)

$$\nu_m = \frac{\alpha_m C_s^2}{\Omega_K} \sqrt{1 + \beta_\phi} \quad (20)$$

- Radial and vertical dependence as given in Bessolaz et al. (2008):

$$\nu_m = \alpha_m \Omega_K H^2 \exp\left[-\left(\frac{z}{H}\right)^4\right], \quad (21)$$

the latter decreasing on a disc scale height $H = C_s/\Omega_K$, here Ω_K is the Keplerian rotation speed. In Eq. (20), β_ϕ is a constant that we fixed to the value 0.1. Throughout this study we will focus in more detail on the resistivity given in Eq. (21), since this expression takes into account the vertical stratification of the accretion disc. We have taken the z -axis parallel to the rotation axis of the disc and assume that the magnetic dipole moment is aligned with the rotational axis.

3 NUMERICAL IMPLEMENTATION

3.1 Code

In order to investigate the disc-star interaction, we use the MHD module provided by PLUTO code version 4.4 (Mignone 2009, Mignone et al. 2007) to perform adiabatic global MHD simulations of accretion discs to numerically solve the MHD equations given in section 2.1. Simulations runs on spherical geometry (R, θ, ϕ) , were performed using the second-order linear reconstruction Runge Kutta integration in time to advance conserved variables. To enhance the stability of the code, in the subroutine `pml_states` we consider the Van Leer limiter in the density and in the magnetic field since is more diffusive, while a monotonized central differences limiter (`minmod`) was used in pressure and velocity fields. Also, we mention that for the inclusion of the cooling term that controls the possible heating of the disc, we have used a power-law cooling option provided in the code. Additionally, inspired by the work of Čemeljić (2019) we use a hll solver with a modification in the `flag_shock` subroutine: flags were set to switch to a more diffusive hll solver when the internal energy defined by $e = P_{\text{gas}}/(\gamma - 1)$ was lower than 1% of the total energy given by the equation (5). Furthermore the condition $\nabla \cdot B = 0$ was maintained using the constrained transport method. Lastly, we mention that in this work we have followed closely the initial conditions in the disc and corona and boundary conditions at the edges of the computational domain as in the works of Čemeljić (2019) and Zanni & Ferreira (2009), in the next subsections we described these conditions in more detail.

3.2 Simulation parameters and units

The parameters of the simulations are the same as were used in the numerical models of the paper I, and were selected to match a set of observed values for the FS CMA stars (Korčáková et al. 2022). More specifically, we fix the mass, radius, initial disc density and the magnetic field of the star to be $M_* = 6M_\odot$, $R_* = 3R_\odot$, $\rho = 1 \times 10^{-13} \text{g cm}^{-3}$ and $B_* = 6.2 \times 10^3 G$. Furthermore we take

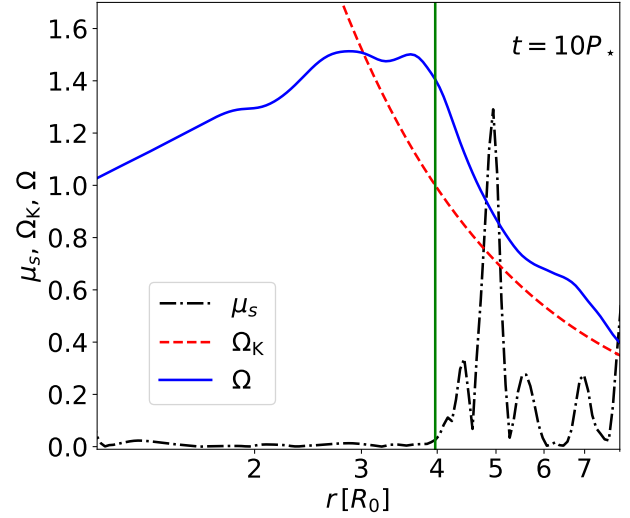


Figure 3. Radial profiles at the midplane of the Sonic Mach number, angular velocity in the disc Ω (normalized by Ω_*) and the Keplerian velocity Ω_K for the BSR0T_1a model calculated at $t = 10P_*$. The green vertical line shows the position of the truncation radius given in Eq. (23).

into account that the aspect ratio is $h = 0.1$. The different models considered are presented in Table 1.

We use the following dimensionless variables:

$$\begin{aligned} R' &= R/R_0 & \rho' &= \rho/\rho_0 & v' &= v/v_{K0} \\ t' &= t/(r_0/v_{K0}) & p' &= p/(\rho_0 v_{K0}^2) & B' &= B/(4\pi\rho_0 v_{K0}^2)^{1/2} \end{aligned}$$

with $R_0 = R_* = 2.087 \times 10^{11} \text{cm}$, $v_{K0} = \sqrt{GM_*/R_0} \approx 6.19 \times 10^7 \text{cm s}^{-1}$, which is the Keplerian velocity at R_0 . For the reference density we take $\rho_0 = 1 \times 10^{-13} \text{g cm}^{-3}$.

In these units, the reference angular rotation rate is $\omega_0 = v_0/R_0 = 2.96 \times 10^{-4} \text{s}^{-1}$, the corresponding timescale is $t_0 = R_0/v_0 \approx 3.37 \times 10^3 \text{s}$ and the rotation period at $R = R_0$, $T_0 = 2\pi t_0 \approx 0.245$ days. For simplicity, we will omit the primes from now on.

Once the initial conditions are normalized, the problem depends on six dimensionless parameters: the aspect ratio h , the equatorial stellar field intensity B_*/B_0 , the stellar rotation rate $\delta_* = R_*\Omega_*/V_{K*}$, the coronal density contrast $\rho_{\text{atm}}/\rho_{d0}$, and the viscous and resistive coefficients α_ν and α_m . Except for the transport coefficients and the initial differential rotation of the star, the other parameters are the same as were used in the simulations of paper I: $h = 0.1$, $B_* = 6200G$, $\rho_{\text{atm}}/\rho_{d0} = 1 \times 10^{-2}$.

3.2.1 Co-rotation and truncation radius

To study the interaction of a star-magnetized disc it is important to identify where the truncation radius must occur by the stellar magnetosphere. So far there are numerous studies that debate the most precise way to determine this radius (see for instance: Romanova et al. 2002; Zanni & Ferreira 2009; Bessolaz et al. 2008; Long et al. 2005). However, despite the differences between all the models, it has been determined that for accretion to occur the truncation radius r_t must be located within the co-rotation radius $r_{\text{co}} = (GM_*/\Omega_*)^{1/3}$. We can rewrite the co-rotation radius in terms of the star radius R_* if we isolate Ω_* variable from the definition of stellar rotation rate δ_* given in the previous section and substitute its value in the definition

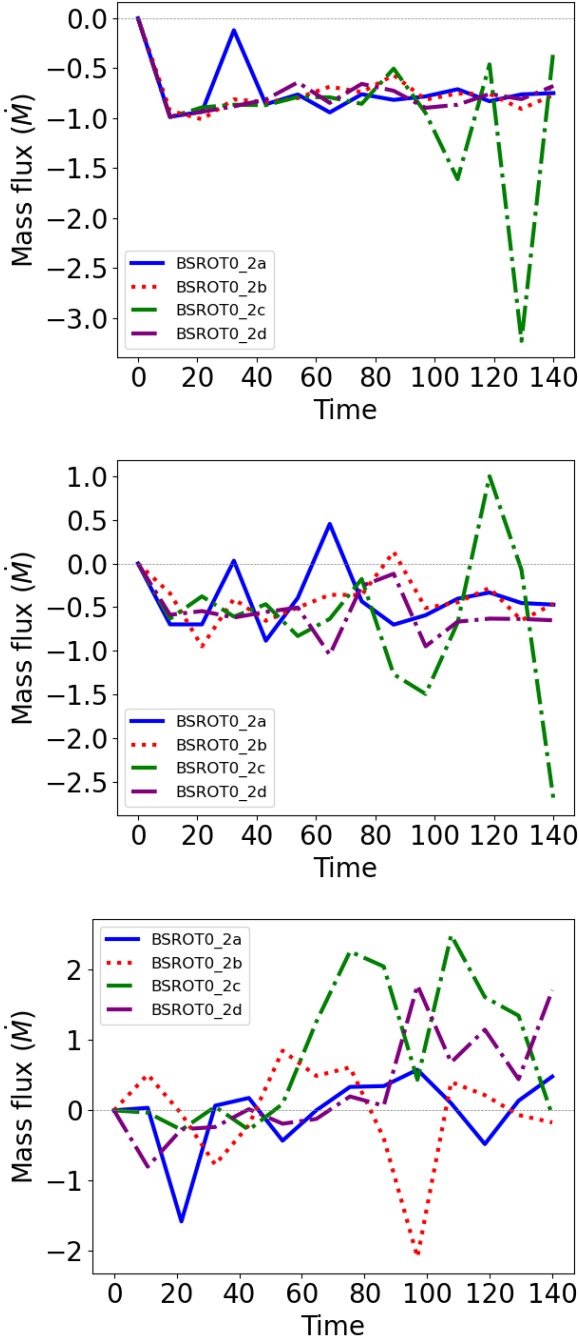


Figure 4. Time dependence of the mass flow rate \dot{M} , for the BSR0T.2 models, calculated at $R = 3.0R_0$ (top panel), $R = 3.96R_0$ (middle panel) and $R = 10R_0$ (bottom panel), respectively.

mentioned above, we will obtain after doing a bit of algebra that the radius of co-rotation can be written as follows $r_{\text{co}} = 4.64R_*$.

On the other hand, we obtained the value for the truncation radius following the next expression (Bessolaz et al. 2008):

$$\frac{r_t}{R_*} \approx 2m_s^{2/7} B_*^{4/7} \dot{M}_a^{-2/7} M_*^{-1/7} R_*^{5/7} \quad (22)$$

considering that the value of m_s can be close to 1 and substituting

the values described in section (3.2) we obtain that:

$$\frac{r_t}{R_*} \approx 3.97121258. \quad (23)$$

It should be emphasized that in the calculation of r_t given in Eq. (23), we have considered an accretion rate $\dot{M} = 10^{-8} M_\odot \text{yr}^{-1}$, which is a conservative value because there is currently debate about what is the correct value of the accretion rate in the FS CMA-type objects (see Carciofi et al. 2010, and references therein).

3.3 Mesh domain

The axisymmetric disc is modeled in the radial range $1R_0 \leq R \leq 30R_0$ with a polar angular extension in one quadrant ($0 \leq \theta \leq \frac{\pi}{2}$). All of our numerical simulations presented here were performed by the same numerical resolution, with a logarithmically increasing grid in radial direction $N_R = 109$ and, $N_\theta = 50$ polar grid cells uniformly distributed. The resulting computational mesh is sufficient to resolve properly the star-disc magnetospheric interaction (SDMI) in both dimensions (see Čemeljić et al. 2017), and in turn allows us to study a larger number of parameters (see Table 1) with a reasonable computational cost.

3.3.1 Boundary Conditions and internal boundary

Since we are interested in analyzing the gas dynamics when SDMI occurs, considering a slow-rotating massive star with strong magnetic field (see subsection 3.2), we take particular care about the boundary conditions implemented on the stellar surface as in previous studies where the SDMI has been analyzed for young stars with a weaker magnetic field (see for instance Romanova et al. 2002, 2009; Zanni & Ferreira 2009; Čemeljić 2019). Then, the boundary conditions that were used in carrying out this work closely follow those described in the works of Zanni & Ferreira (2009) and Čemeljić (2019).

To obtain adequate gas dynamics on the surface of the star, we implement the following conditions. First, in the reference frame co-rotating with the star, the electric field is zero (see equation (11) in Zanni & Ferreira 2009, for details). Second, to prevent low-density near the star, we modified the density value when it falls below some limit value¹ within a grid cell of the computational domain on the surface of the star. For the corona region, to conserve the same sound speed and to keep the conservation of the momentum we modify the gas pressure and the velocities, respectively. Lastly, to follow the evolution of the disc, we activate the scalar tracer, taking a value of unity in the disc domain and zero outside of it. Note that because the resistivity described in the equations (19)-(21) is only applied within the domain of the disc mesh, the reconnection of the magnetic field arising in the magnetosphere is handled by numerical dissipation.

For the inner grid ghost cells, following Čemeljić (2019) we prescribe the values of the density, pressure, and toroidal components of the velocity and magnetic field from the active zones. This implies that the density and the magnetic field are linearly extrapolated considering a Van Leer limiter, and minmod limiter in the pressure and velocity (see subsection 3.1). It should be emphasized that to achieve numerical stability in the corona, when $v_R > 0$ in the inner radial boundary, we define the gas pressure as $P = (2/5 - T_f v^2) \rho_c R^{-5/2}$, with T_f a free parameter (see Čemeljić 2019).

On the other hand, in the radial outer boundary condition, we

¹ The low-density limit used here is $\rho = 5 \times 10^{-8}$ in code units, similar to the value used in Čemeljić (2019).

consider the outflow condition for the velocity components, and for the density and magnetic field a linear extrapolation was used. Lastly, in the θ -direction we use the PLUTO code options 'axisymmetric' and 'eqtsymmetric' for the boundary conditions at $\theta = \theta_{\min}$ and $\theta = \theta_{\max}$, respectively, since we simulate only one hemisphere of the disc.

4 RESULTS

In this section we present the results of our 2.5D-MHD simulations of a resistive accretion disc for different values of α_ν and α_m , and also considering different stellar rotation rates. Our study is focused on the strong magnetic field regime measured in massive stellar objects such as FS CMA-type stars (see [Korčáková et al. 2022](#)).

All the parameters and the different models are given in the table 1. The viscosity parameter describes the strength of the viscous torque, that allows the disc to accrete, while the resistivity parameter α_m allows coupling of the stellar magnetic field with the disc material.

For both viscosity and resistivity we consider the pair of values of 0.1 and 1. So the Prandtl number can take the set of values of $P_m = \{0.06, 0.6, 6.6\}$. The motivation for choosing these values in the viscosity lies in the fact that previous studies of the star-disc interaction show that if it is fulfilled $\alpha < \alpha_{\text{crit}} \approx 0.685$, a backflow is originated in the mid-plane of the disc, which results in the accretion of the disc towards its surface (see [Zanni & Ferreira 2009](#), and references therein).

On the other hand, the choice of values 0.1 and 1 for the α_m resistivity coefficient, are motivated to know which region of the disc is steadily connected to the star in our models with a strong magnetic field. Since the opening of the magnetosphere is intrinsically driven by the differential rotation between the disc and the star, as well as with the resulting buildup of toroidal magnetic pressure. The latter can be modified by the value that α_m takes on the disc, since if $\alpha_m = 1$ limits the growth of a toroidal magnetic field, producing a larger connected region (an extended magnetosphere). In the case when $\alpha_m = 0.1$ it has the opposite effect on the magnetic pressure (due to the strong coupling), thus producing a smaller connected region (compact magnetosphere).

4.1 Comparison of the stellar rotation rate for models with an extended magnetosphere

Figure 1 shows a comparison between the BSROT0.1b and BSROT0.2b models. In these models the only difference in the parameters is a factor of 2 in the rate of stellar rotation δ_\star . We find that in the case of a slower stellar rotation (BSROT0.1b model) it produces an accretion towards the star in the mid-plane of the disc as well as a distribution of the gas of the disc outside the mid-plane that resembles the formation of the funnel effect that can give rise to accretion near the poles. Also, we find in this case the formation of disc winds and magnetospheric ejections. In the case of T Tauri stars with a smaller magnetic field on the star's surface ($B_\star = 1.1kG$) a similar behavior has been found in the formation of the funnel effect and in the generation of magnetosphere ejections (see [Zanni & Ferreira 2013](#)). However, in said study there are no signs of gas accretion in the mid-plane of the disc. In the case of a star rotating a little faster (case described here by the BSROT_2b model), we find an inflation of the disc, which is the result of the inflation and reconnection of the magnetic field lines, in addition to the fact that we find the formation of layers between $r = 5R_0$ and $r = 10R_0$.

These layers fail to form multiple funnels towards the star due to the increase in the rotation of the star.

4.2 Models with compact and extended magnetospheres with the same stellar rotation rate

In the Fig. 2 we show the logarithmic gas density maps for the BSROT0.1a and BSROT0.1b models calculated at $t = 60P_\star$. In the first case, we find that in a disc with lower magnetic diffusivity ($\alpha_m = 0.1$) there is a formation of two knots at $R = 17$ and $R = 25R_0$. The first knot creates strong disturbances in the density of the disc, producing a partial gap in $R = 17R_0$. The second knot located outside the mid-plane of the disc (at $R = 25R_0$) generates a magnetosphere ejection. For the BSROT0.1b model with a higher resistivity ($\alpha_m = 1$), we find the formation of a single knot outside the mid-plane of the disc at $R = 13R_0$ which produces a magnetosphere ejection. In both models we find that the gas accretion takes place in the mid-plane of the disc. We emphasize that, since the stellar rotation rate in these models is the same, it is clear that the differences in the gas density distribution arise due to the value of the resistivity within the disc.

Figure 3 shows the radial profiles of the sonic Mach number $\mu_s = |u_r|/\sqrt{P/\rho}|_{z=0}$, the disc angular velocity Ω and the Keplerian velocity Ω_K , respectively (normalized by Ω_\star), calculated at $t = 10P_\star$ for the BSROT0.1a model. The behavior of the dynamics in the disc is changing the accretion Mach number which increases and reaches a maximum value of $\mu_s \approx 1.3$ in a radius of $5R_0$ (see Fig. 3). Note that μ_s starts to increase outward from the truncation radius r_t (green vertical line in Fig. 3). On the other hand, we can see in Fig. 3 that the angular velocity of the disc Ω becomes super-Keplerian for $R > 3.1R_0$ (solid blue line). This implicitly means that the rotating star exerts a positive torque on the disc. In other words, the star loses angular momentum which consequently translates into a lower rotation speed of the star. Although in this case, the magnetic field is strongly coupled to the disc (since $\alpha_m = 0.1$), we point out that we find very similar results in cases when the resistivity is higher ($\alpha_m = 1$). Therefore, if the magnetic field is able to couple to the disc, the rotation speed of the star will inevitably decrease. The latter may explain why FS CMA-type stellar objects as IRAS 17449+2320 with a strong magnetic field exhibit a very low stellar rotation rate.

4.2.1 Magnetospheric ejections

In previous studies of disc models that include a compact magnetosphere ($\alpha_m = 0.1$) and a weak magnetic field, magnetospheric ejections have been found ([Zanni & Ferreira 2013](#); [Čemeljić 2019](#); [Čemeljić et al. 2023](#)). This type of coronal ejections can substantially modify the stellar rotation depending on the strength of the magnetic field and can produce a spin-down of the star ([Čemeljić et al. 2023](#)). Remarkably, we find magnetospheric ejections in both disc models with a compact and with an extended magnetosphere (that is, $\alpha_m = 0.1$ and $\alpha_m = 1.0$, see for instance Fig. 2). We think that in the case of FS CMA-type stars the observed low-stellar rotation is produced by such magnetospheric ejections and, therefore, definitely deserves a detailed investigation which is beyond the scope of this study and should be studied elsewhere.

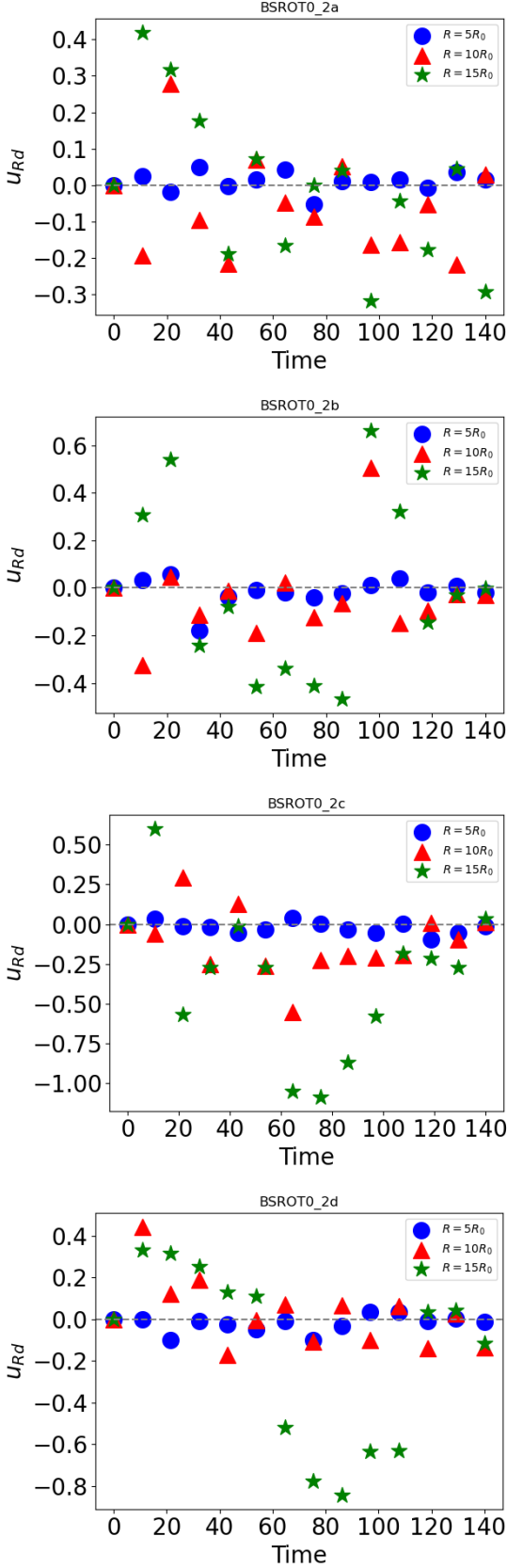


Figure 5. Radial velocity in the mid-plane as a function of time, calculated at three different points $R = 5R_0$, $R = 10R_0$ and $R = 15R_0$. In all graphs presented has been considered that the rate of stellar rotation is $\delta_\star = 0.2$. The corresponding model is indicated at the top of each subplot.

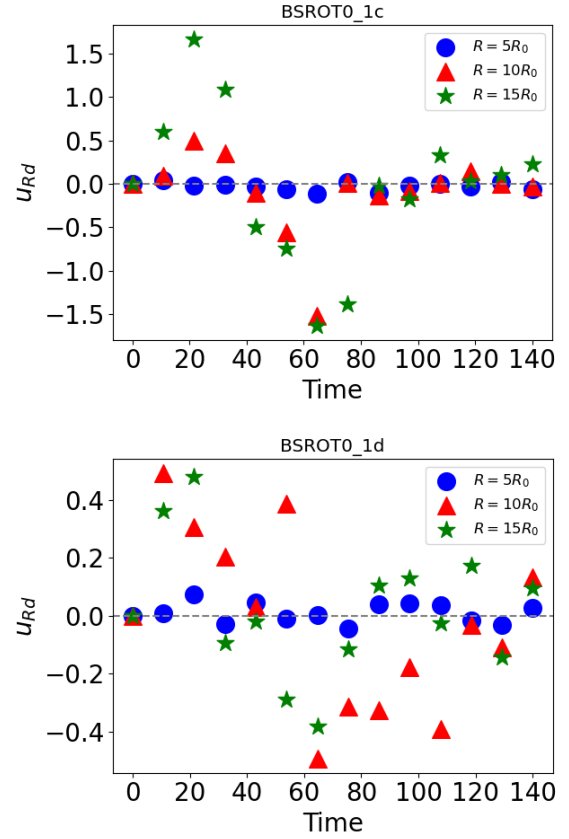


Figure 6. Radial velocity at the mid-plane as a function of time, calculated at three different points $R = 5R_0$, $R = 10R_0$ and $R = 15R_0$. In all graphs presented has been considered that the rate of stellar rotation is $\delta_\star = 0.1$. At the top of each subplot the model to which it corresponds is indicated.

Model	$\Omega_\star/\Omega_{\text{br}}$	$P_\star(\text{days})$	α_ν	α_m	P_m
CSROTO_1a	0.1	4.6	1.0	0.1	0.6
CSROTO_1b	0.1	4.6	1.0	1.0	0.6
MSROTO_1a	0.1	4.6	1.0	0.1	0.6
MSROTO_1b	0.1	4.6	1.0	1.0	0.6
BSROTO_1a	0.1	4.6	1.0	0.1	6.6
BSROTO_1b	0.1	4.6	1.0	1.0	0.6
BSROTO_1c	0.1	4.6	0.1	0.1	0.6
BSROTO_1d	0.1	4.6	0.1	1.0	0.06
BSROTO_2a	0.2	2.3	1.0	0.1	6.6
BSROTO_2b	0.2	2.3	1.0	1.0	0.6
BSROTO_2c	0.2	2.3	0.1	0.1	0.6
BSROTO_2d	0.2	2.3	0.1	1.0	0.06

Table 1. Parameters of our numerical models. *First column.* Name of each model, the first letter indicates what type of magnetic diffusivity was used (B: Bessolaz, C: Classic and M: Modified, respectively). *Second column.* The stellar rotation rate. *Third column.* Rotation period of the star. *Fourth column.* The anomalous viscosity coefficient. *Fifth column.* Dimensionless coefficient of magnetic diffusivity. *Sixth column.* Prandtl number defined as $P_m \equiv 2\alpha_\nu/3\alpha_m$.

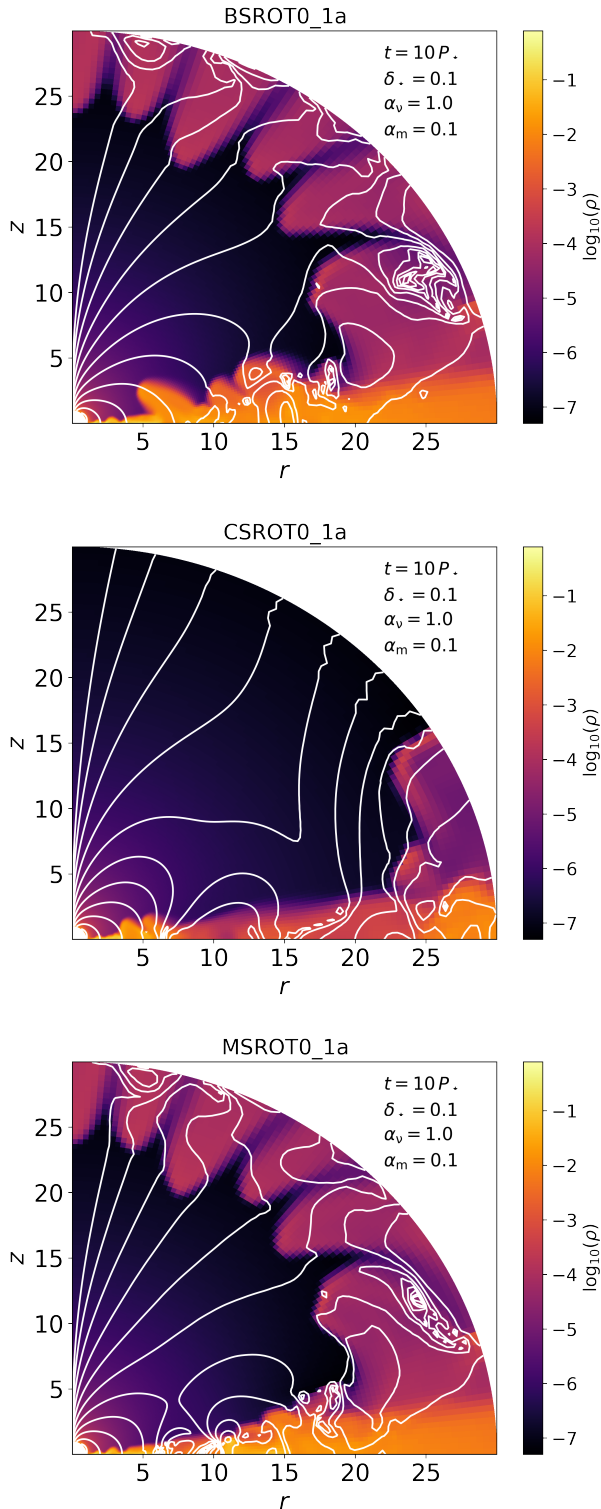


Figure 7. Comparison between different models. In this figure we show the results using a time period of $10P_\star$, with a low stellar rotation rate $\delta_\star = 0.1$, and a low magnetic diffusivity $\alpha_m = 0.1$ using the three different descriptions to obtain the resistivity discussed in section 2.5. The logarithmic gas density (color-scale background) changes from maximum value $\rho = -0.1$ in the disc to the minimum value $\rho = -7.3$ in the corona. The white lines show the poloidal magnetic field lines.

5 DISCUSSION

5.1 The mass flow

The mass flow rate crossing the whole domain is the integral of the mass flux inside and outside of the disc. It is given by

$$\dot{M} = -4\pi R^2 \int_0^{\pi/2} \rho u_{Rd} \sin \theta d\theta. \quad (24)$$

Figure 4 shows the mass flow rate for four models (BSROTO_2a, BSROTO_2b, BSROTO_2c and BSROTO_2d), calculated at three different radius of the disc. The upper panel corresponds to $R = 3.0R_0$. We find that for the four models the rate of mass flux towards the central star is always negative or zero with values between zero to -0.3. This behaviour was expected since in that part there is not formation of strong outflows (see figure 1 bottom panel). Also this means that there is no inflow of gas towards the central star in the mid-plane of the disc. The middle panel in Fig. 4 corresponds to the value given in equation (23) truncation radius $R = 3.97R_0$. We can see some positive values in the models BSROTO_2a, BSROTO_2b and BSROTO_2c. In the bottom panel in Fig. 4 we show the case when $R = 10.0R_0$. Here we can see that for the models BSROTO_2c and BSROTO_2d the mass flux rate becomes positive after a time of $t = 60T_0$ and $t = 70T_0$, respectively, which means that the accretion disc stops at a radius greater than $R = 10.0R_0$.

5.2 Backflow and radial velocity

Under some conditions, a phenomenon known as "backflow" occurs in the accretion disc (see Mishra et al. 2023, and references therein). This phenomenon appears when a part of the disc flow moves in the opposite direction, away from the central object and usually appears in the mid-plane of the disc. In the figure 5 we show the radial velocity for the models where the resistivity was obtained using the description given in Eq. (21) and considering the case when the rate of stellar rotation is $\delta_\star = 0.2$.

In the plots we show the temporal evolution of the radial velocity component calculated at three different radii. The blue circles correspond to $R = 5R_0$, the red triangles to $R = 10R_0$ and the green stars symbols correspond to $R = 15R_0$. In the four models we can observe that when the radial velocity is calculated in a radius corresponding to $R = 5R_0$ the radial velocity is approximately zero over time. However, when the radius is taken as $R = 10R_0$ or $R = 15R_0$ we find negative values for the radial velocity component. That means an intermittent backflow appears as a function of the time, i.e., that backflow persists for certain time intervals and disappears in others.

On the other hand, for a stellar rotation rate of $\delta_\star = 0.1$, considering a compact and extended magnetosphere (BSROTO_1c and BSROTO_1d models) we find again an intermittent backflow when we analyze the radial component of the velocity at radial distances from the star of $R = 10R_0$ and $R = 15R_0$, as can be seen in the figure 6. It is important to point out that although in most of the BSROTO_1 and BSROTO_2 models the magnetic Prandtl number P_m , is close to (or exceeds) the critical value of the Prandtl number ($P_m^{\text{crit}} \approx 0.6$; see Mishra et al. 2023), we find intermittent backflow at the mid-plane of the disc. Therefore, our results support the argument given in Mishra et al. (2023) that the backflow is a physical effect rather than a numerical effect.

5.3 Observed disc structure in FS CMa stars

There are several observational studies in which the presence of thick disc structures around FS CMA-type stars has been suggested. For example, the analysis of FS CMA interferometric data by Hofmann et al. (2022) shows that the outer dust ring has an inclination angle of approximately 40° . However, in the UV spectra a strong absorption of elements from the iron group is detected, indicating an enormous amount of gas at these angles. Among other common properties of these objects, the presence of expanding layers, which can slow down, has also been suggested (Kučerová et al. 2013). Clumps moving away from the star were detected in Jeřábková et al. (2016) and evidence of material infall in Kučerová et al. (2013). Another important effect was reported by Ellerbroek et al. (2015). Based in the interferometric observations of HD 50138 in $B\gamma$ with AMBER. They found that the star HD 50138 is surrounded by an au-scale rotating gas disc and spherical halo. Among some of the results they reported are that the radius of the outer disc is 0.6au, the radius of the halo is 3au, and Δv in the halo is 60km/s. The results shown in our figure (7) can explain observed phenomena reported by Ellerbroek et al. (2015). The models BSROT0_1a and MSROT0_1a show that the structure of the disc is thicker and also we can observe a structure on the edge that could be explained as a halo surrounding the disc.

Another study that supports the idea that FS CMA-type stars are surrounded by thick disc was done by Zickgraf & Schulte-Ladbeck (1989). They found that the FS CMA stars are surrounded by a very extended and optically thick disc. Based on polarimetric observations at Calar-Alto, they found that the disc opening angle is $\approx 30^\circ$ for the stars MWC 645 and MWC 939. We find that in all our models there is an increase in the aspect ratio as it evolves over time. For instance, in the case of the BSROT0_1b model the aspect ratio increased 3.5 times for a corresponding time of $P_\star = 130$ stellar periods that means that in this case we found that the disc opening angle is $\approx 25^\circ$, while for the BSROT0_2b model the disc opening angle is $\approx 33^\circ$ i.e. the aspect ratio increased 4.6 times for the same time period. In Fig. 1 one can see how the disc is thickened.

5.4 Magnetic field configuration inside the accretion disc

In the case of a compact magnetosphere (models with $\alpha_m = 0.1$), we find that the magnetic field configuration is far from the standard configuration of a vertical magnetic field (resulting from an initial dipole configuration). We find that the poloidal magnetic field lines are twisted (see for example Fig.2). In such configuration, the magnetic reconnection heating the corona is highly probable, that could explain the presence of the weak Raman lines found observationally in several FS CMA stars. Additionally, we can see in the upper panel in Fig. 2 that the magnetic field lines within the disc inflate and twist rapidly (within the first 10 orbital periods of the star), which gives rise to the formation of knots at different radial distances near the disc mid-plane. These knots substantially modify the density of the disc producing regions of low density. In other words, they can generate the formation of shallow gaps in the disc which can be displaced radially depending on the inflation rate of the magnetic field lines (see upper panel in Fig. 7). In addition, the knots can also move towards the corona region, dragging gas with them from the surface of the disc, so the disc suffers a thickening. It should be emphasized that regardless of the analytical form of the magnetic diffusivity described by equations (19-21), when $\alpha_m = 0.1$ we find the formation of at least a pair of knots tied to the mid-plane of the disc. This result implies the generation of strong turbulence

within the disc which can modify the velocity components and the density distribution.

On the other hand, when $\alpha_m = 1$ we find that the formation of knots occurs in the corona region near the disc layer (see lower panel in Fig. 2), and therefore the perturbations in density and velocities within the disc are smaller. However, these perturbations produce a higher accretion rate in the mid-plane of the disc (see below) unlike other studies where strong magnetic fields are also considered (Miller & Stone 1997; Romanova et al. 2002; Čemeljić et al. 2023). We think that the main reason for obtaining a greater perturbation in density within the disc is due to the vertical dependence of the density. Since we use a vertical profile of the density that depends on the height through the polar θ -coordinate and, therefore the density of the disc decays for values of θ close to the aspect ratio of the disc h and facilitates the inflation of the magnetic lines. Otherwise, as shown in Čemeljić et al. (2023) when a density-taper function ($\rho = \rho_c r^{-3/2}$) in the corona-disc interface region is used, the density becomes more noisy there without drastic density changes near the mid-plane since the magnetic field decreases by at least two orders of magnitude.

6 SUMMARY AND CONCLUSIONS

We have performed a set of 2.5D magnetohydrodynamical simulations to analyze the star-disc interaction of FS CMA type stellar objects that exhibit a strong magnetic field at the star surface ($B_\star = 6.2kG$; Korčáková et al. 2022). Based on the results of Paper I we set the value of the disc density $\rho_{d0} = 10^{-13} \text{gcm}^{-3}$, and we have considered as free parameters; the viscosity α_v , and the resistivity α_m inside of the accretion disc, as well as the stellar rotation rate δ_\star . By varying the resistivity, we analyze the effect of the magnetic field on the density of the disc and the corona region in the cases of a compact ($\alpha_m = 0.1$) and extended magnetosphere ($\alpha_m = 1$), respectively.

We find that a higher stellar rotation rate ($\delta_\star = 0.2$) can modify the density structure in the internal region of the disc, generating different layers when $R \leq 10R_0$, which adds to the effect generated by a higher viscosity ($\alpha_v = 1$) that produces the thickening of the accretion disc. In the case of a low-viscosity ($\alpha_v = 0.1$), we find that in both models star-disc interaction with a compact or extended magnetosphere the fall of gas towards the star can be in the mid-plane. However, we do not rule out that the funnel effect may occur where the accretion of gas is conducted near the star's poles, since until the end of our simulations, the density structure in most of our models resembles a form similar to the funnel effect reported in less massive stars with a lower magnetic field (see for instance Romanova et al. 2002; Bessolaz et al. 2008; Zanni & Ferreira 2009, 2013; Čemeljić 2019).

On the other hand, since we consider a value of $\alpha_v = 0.1 < 0.685$, we have analyzed if there is a backflow in the mid-plane of the disc which was previously reported (see Čemeljić 2019, and references therein). We find that regardless of the type of magnetosphere modeled there is intermittent backflow, as well as several knots forming in the magnetic field lines near and in the mid-plane of the disc. These knots produce perturbations in the density and velocity components, as well as the formation of shallow gaps in the density whose position depends on the inflation of the magnetic field lines.

Furthermore, we conclude that our findings may have direct implications for understanding the observational results for the study of post-mergers among FS CMA stars, because as we can see in our simulations the disc structure changes and becomes thicker significantly. Our simulations could also explain some other

properties that have been found observationally in FS CMA stars (Kučerová et al. 2013), such as: material outflow and inflow, the formation of layers, and also the presence of the weak Raman lines found in several FS CMA stars than can be explained by corona heating due to the magnetic reconnection.

ACKNOWLEDGEMENTS

We thank the referee for his/her thorough reading of our manuscript, and for his/her constructive and careful report, which helped us improve the previous version of this work. This work was supported by the Czech Science Foundation (grant 21-11058S). The work of ROC was supported by the Czech Science Foundation (grant 21-23067M). Computational resources were available thanks to the Ministry of Education, Youth and Sports of the Czech Republic through the e-INFRA CZ (ID:90254).

DATA AVAILABILITY

The PLUTO code is available from <http://plutocode.ph.unito.it>. The input files for generating our 3D magnetohydrodynamical simulations will be shared on reasonable request to the corresponding author.

REFERENCES

- Bessolaz N., Zanni C., Ferreira J., Keppens R., Bouvier J., 2008, *A&A*, 478, 155
- Carciofi A. C., Miroshnichenko A. S., Bjorkman J. E., 2010, *ApJ*, 721, 1079
- Ellerbroek L. E., et al., 2015, *A&A*, 573, A77
- Hofmann K. H., et al., 2022, *A&A*, 658, A81
- Ireland L. G., Zanni C., Matt S. P., Pantolmos G., 2021, *ApJ*, 906, 4
- Jeřábková T., et al., 2016, *A&A*, 586, A116
- Kluźniak W., Kita D., 2000, *arXiv e-prints*, pp astro-ph/0006266
- Kluźniak W., Rappaport S., 2007, *ApJ*, 671, 1990
- Koldoba A. V., Lovelace R. V. E., Ustyugova G. V., Romanova M. M., 2002, *AJ*, 123, 2019
- Korčáková D., et al., 2022, *A&A*, 659, A35
- Kučerová B., et al., 2013, *A&A*, 554, A143
- Křiček R., et al., 2017, in Miroshnichenko A., Zharikov S., Korčáková D., Wolf M., eds, *Astronomical Society of the Pacific Conference Series Vol. 508, The B[e] Phenomenon: Forty Years of Studies*. pp 411–412
- Long M., Romanova M. M., Lovelace R. V. E., 2005, *ApJ*, 634, 1214
- Masoumeh S., Khesali A., 2022, *ASJ*, 75, 18
- Mignone A., 2009, *Memorie della Societa Astronomica Italiana Supplementi*, 13, 67
- Mignone A., Bodo G., Massaglia S., Matsakos T., Tesileanu O., Zanni C., Ferrari A., 2007, in *JENAM-2007, “Our Non-Stable Universe”*. pp 96–96
- Miller K. A., Stone J. M., 1997, *ApJ*, 489, 890
- Mishra R., Čemeljić M., Kluźniak W., 2023, *MNRAS*, 523, 4708
- Moranchel-Basurto A., Korčáková D., Chametla R. O., 2023, *Monthly Notices of the Royal Astronomical Society*
- Powell K. G., Roe P. L., Linde T. J., Gombosi T. I., De Zeeuw D. L., 1999, *Journal of Computational Physics*, 154, 284
- Romanova M. M., Ustyugova G. V., Koldoba A. V., Lovelace R. V. E., 2002, *ApJ*, 578, 420
- Romanova M. M., Koldoba A. V., Ustyugova G. V., Kulkarni A. K., Long M., Lovelace R. V. E., 2009, in Pogorelov N. V., Audit E., Colella P., Zank G. P., eds, *Astronomical Society of the Pacific Conference Series Vol. 406, Numerical Modeling of Space Plasma Flows: ASTRONUM-2008*. p. 112 ([arXiv:0901.4269](https://arxiv.org/abs/0901.4269)), doi:10.48550/arXiv.0901.4269
- Tanaka T., 1994, *Journal of Computational Physics*, 111, 381
- Zanni C., Ferreira J., 2009, *A&A*, 508, 1117

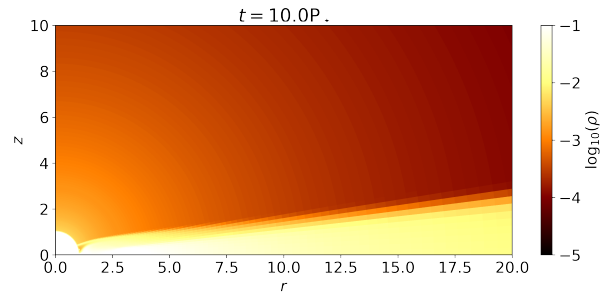


Figure A1. Density in the hydrodynamic model in logarithmic scale in units of ρ_0

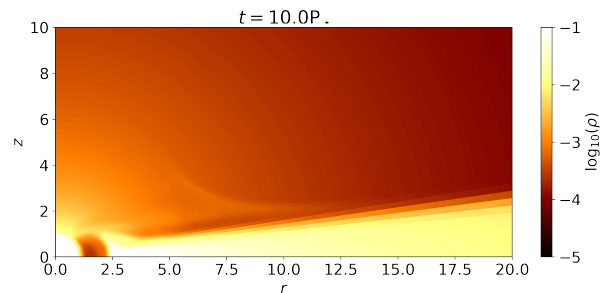


Figure A2. Density in the magnetohydrodynamical model in logarithmic scale in units of ρ_0

- Zanni C., Ferreira J., 2013, *A&A*, 550, A99
- Zickgraf F. J., Schulte-Ladbeck R. E., 1989, *A&A*, 214, 274
- Čemeljić M., 2019, *A&A*, 624, A31
- Čemeljić M., Parthasarathy V., Kluźniak W., 2017, in *Journal of Physics Conference Series*. p. 012028 ([arXiv:1802.00261](https://arxiv.org/abs/1802.00261)), doi:10.1088/1742-6596/932/1/012028
- Čemeljić M., Kluźniak W., Parthasarathy V., 2023, *A&A*, 678, A57

APPENDIX A: FUNNEL EFFECT IN LOW-MAGNETIZED STARS: SET-UP COMPROBATION

A1 Test code for low-magnetized stars

In Figure A1 we show the results of gas density at $t = 10P_*$ obtained from the simulations considering the hydrodynamic case (i.e. without magnetic field) and a rotation of the star of 0.1. It is clearly observed that the material is being accreted towards the center. On the other hand in fig. A2 we show the results obtained from the simulations considering the magnetohydrodynamic case for a star with a rotation of 0.1, in this case we used a weak magnetic field ($B_* = 140G$) in order to see if our results are in agreement with others studies where they report the occurrence of the funnel effect in T-Tauri stars. In fig. A2 we shown the gas density distribution of our numerical test where we can see that from early times ($t = 10P_*$) the funnel effect is already formed. This means, that the matter flows out of the disc plane and essentially free-falls along the stellar magnetic field lines. Therefore, our results are in agreement with what was previously reported by Zanni & Ferreira (2009), Romanova et al. (2002), Čemeljić (2019).

This paper has been typeset from a \LaTeX file prepared by the author.